

Article

Research on High-Pressure Water Jet Interference for Collision Prevention of Waterway Viaduct Piers: Case Study of Guangzhou Lixinsha Bridge

Jincai Chen, Xiquan Wei, Jingjing Huang, Haibo Wang and Meiling Dai *

School of Civil and Transportation Engineering, Guangdong University of Technology, Guangzhou 510006, China; chenjc@gdut.edu.cn (J.C.); wxq1619@163.com (X.W.); 13684804265@163.com (J.H.); wanghaibo@gdut.edu.cn (H.W.)

* Correspondence: meiling-dai@163.com

Abstract: In this paper, with the frequent occurrence of ship–bridge collision accidents as the context and the collision accident of the Lixinsha Bridge in China as the background, the scenario of a ship impacting a pier was simulated using ANSYS-FLUENT software, and the practical application possibility of the high-pressure water jet interference (HPWJI) anti-collision method was thoroughly investigated. Through the simulation analysis, the effectiveness of a high-pressure water jet with a total flow rate of 45 m³/s in altering the navigation direction of large-tonnage (2000 t) ships and avoiding obstacles was verified. Additionally, its impact on the stress of the ship steel plates and navigation status was also explored. It was found that, with reasonable layout and parameter adjustment, the high-pressure water jet technology could effectively intervene in the ship’s navigation trajectory while ensuring the structural safety of the ship, with minimal impact on the ship’s navigation stability and passenger comfort. Furthermore, the injection angle of the high-pressure water jet had a significant impact on the deflection and deceleration of the ship. Specifically, when the water jet impacted the ship along its forward direction, it could effectively increase the ship’s deceleration and deflection time, reducing the speed from 2.55 m/s to 1.7 m/s, a decrease of approximately 33%, significantly enhancing collision prevention effectiveness. This research provides important guidance for the practical application of high-pressure water jet collision prevention technology and is of great significance for improving the safety of waterway transportation.

Citation: Chen, J.; Wei, X.; Huang, J.; Wang, H.; Dai, M. Research on High-Pressure Water Jet Interference for Collision Prevention of Waterway Viaduct Piers: Case Study of Guangzhou Lixinsha Bridge.

Buildings **2024**, *14*, 2118. <https://doi.org/10.3390/buildings14072118>

Academic Editor: Bartolomeo Pantò

Received: 5 June 2024

Revised: 1 July 2024

Accepted: 7 July 2024

Published: 10 July 2024



Copyright: © 2024 by the authors. Submitted for possible open access publication under the terms and conditions of the Creative Commons Attribution (CC BY) license (<https://creativecommons.org/licenses/by/4.0/>).

Keywords: ship–bridge collision; fluid–structure interaction; collision prevention measures; high-pressure water jet

1. Introduction

With the booming development of the global economy, the demand for water transportation is growing day by day, resulting in an increasing density of shipping routes. To promote cultural exchange and economic growth, numerous cross-sea and cross-river bridges have been constructed to shorten transportation distances. However, this trend has also brought about a non-negligible issue: the frequent occurrence of ship–bridge collisions. The increase in shipping routes and the number of bridges has significantly elevated the risk of ship–bridge collisions [1], posing a significant threat to people’s lives and property safety.

In recent years, ship–bridge collisions have been a common occurrence, not only causing severe casualties and significant economic losses but also adversely affecting social stability and economic development [2–4], as exemplified by the recent collision incident involving the Lixinsha Bridge in Guangzhou. The accident resulted in five deaths and three injuries, causing great shock to the local community. Therefore, how to effectively prevent ship–bridge collisions and ensure the safety of waterway transportation has

become a key issue of concern for both the international academic and engineering communities.

As a crucial means to address this issue, the research and development of ship–bridge collision prevention technology are of great significance. This technology mainly covers two major areas, active collision prevention and passive collision prevention [5], aiming to effectively reduce the risk of ship–bridge collisions by optimizing ship navigation management and trajectory planning, and innovating the design of pier collision prevention devices.

Active collision prevention technology focuses on optimizing ship navigation management and trajectory planning, aiming to effectively reduce the risk of ship–bridge collisions through scientific scheduling and precise control. In this field, significant results have been achieved by domestic and foreign scholars, with various effective collision prevention schemes and measures being proposed. For example, utilizing mature radar systems and Automatic Identification System (AIS) for ships [6–8], the real-time monitoring and early warning of ship navigation status can be achieved. When potential collision risks are detected, the system can quickly respond, providing timely and accurate warning information to the crew to assist them in taking countermeasures to avoid collision risks. In addition, bridge photoelectric warning systems based on image recognition technology [9], ship collision warning systems that comply with international maritime collision avoidance rules [10,11], and active collision avoidance algorithms for inland river ships [12] all provide timely and accurate warning information to the crew through an intelligent analysis of ship dynamics and intentions, helping them formulate safer and more efficient navigation plans.

Although active collision prevention technology plays a significant role in reducing the risk of ship–bridge collisions, its effectiveness is limited by the crew’s reaction speed and operational accuracy. In cases of crew violations or operational errors, relying solely on active collision prevention technology may not fully guarantee safety. Therefore, the research and development of passive collision prevention technology are equally crucial.

Compared to active collision prevention technology, passive collision prevention technology focuses on the innovative design of pier collision prevention devices. These devices absorb or disperse the kinetic energy of ships during collisions, thus reducing damage to piers. From early pioneering research [13] to today’s in-depth exploration, passive collision prevention technology has made significant progress in materials, forms, and structures. For example, the application of new materials such as composite sandwich structures [14,15] and glass fiber-reinforced polymer (GFRP) laminates [16,17] has effectively improved the performance and effectiveness of collision prevention devices. At the same time, innovative designs such as ellipsoidal pier collision prevention airbags [18] and large composite bumper collision prevention systems [19–22] have also demonstrated their excellent energy absorption properties through experiments and simulations. These devices can quickly come into play during collisions, effectively reducing damage to piers and reducing accident losses.

However, passive collision prevention technology also has some limitations. Firstly, even with the use of high-performance collision prevention devices, internal bridge damage may not be completely avoided during collisions with large-tonnage ships. Secondly, the collision prevention devices themselves may also suffer significant damage during collisions, requiring regular replacement and maintenance. Additionally, the design and implementation of passive collision prevention technology need to consider various factors such as ship type, navigation speed, and impact angle, which makes it more challenging.

Therefore, we need to explore more comprehensive and effective ship–bridge collision prevention technologies from new perspectives and ideas. In a previous study [23], we proposed a collision prevention concept based on fluid dynamics, which utilizes high-pressure water jets to intervene in the water flow structure, thereby altering the ship’s navigation trajectory or impact angle to achieve collision prevention. For more detailed

information on the interaction mechanism between the water flow and the ship regarding this method, please refer to that study, as it will not be repeated here. This innovative idea provides us with new research directions and ideas. This article will take the Lixinsha Bridge collision incident as an example to analyze the potential and advantages of this fluid dynamics-based collision prevention method in practical applications. Through a theoretical validation and experimental analysis of this method, we aim to provide a new perspective and reference for the research and development of ship–bridge collision prevention technologies.

2. Construction and Parameter Setting of Computational Fluid Dynamics Model

2.1. Definition of Geometric Model and Watershed Boundary

The Lixinsha Bridge collision incident is a highly representative inland waterway collision accident, with its root cause being the distracted navigation of the crew. The vessel involved has a tonnage of up to 2200 tons, fully complying with the conventional standards for inland waterway cargo ships, and the pier has been equipped with traditional anti-collision devices [24]. However, unfortunately, these safety measures failed to fully exert their intended protective effects due to the negligence of the crew, ultimately resulting in severe damage to the pier. Therefore, a thorough investigation of this accident case holds significant referential value for exploring the importance and practical application of the new high-pressure water column anti-collision technology.

Taking the Hongqili Waterway in Guangzhou as the background, a geometric model of the ship–bridge collision scenario based on the river conditions of an annual average flow rate of 1.2 m/s was constructed. The ship type was selected from the type of ship involved in the collision accident on Lixinsha Bridge on 22 February 2024, with detailed parameters listed in Table 1. The geometric model accurately restored the shape and structure of the ship, as shown in Figure 1.

Table 1. Ship model parameters.

Parameter	Value
Length (m)	60
Width (m)	18
Height (m)	6
Draft depth (m)	2.6
Weight (ton)	2200

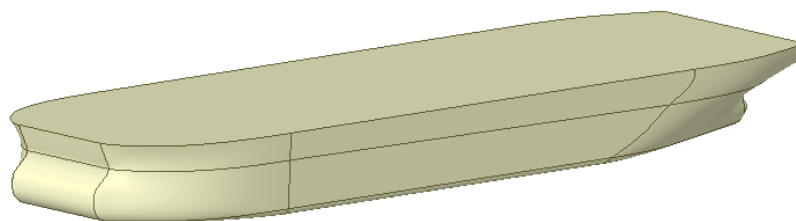


Figure 1. Geometric model of hull.

During the simulation of collision accidents, special consideration was given to the deviation caused by operational errors of the crew. As the ship approached the Lixinsha Bridge, it suddenly made a sharp right turn, and its bow collided with the pier on the right side of the navigation hole at a 35° angle and a speed of 4.6 knots, causing severe damage to the pier, as shown in Figure 2c. The entire computational domain encompassed multiple elements including the piers, ship, air, water flow, and jet sources, with dimensions set as 245 m by 115 m by 55 m. The overall layout is shown in Figure 2. The spacing

between the two piers was 55 m, and the pier foundation structure was modeled with fine detail based on the actual design.

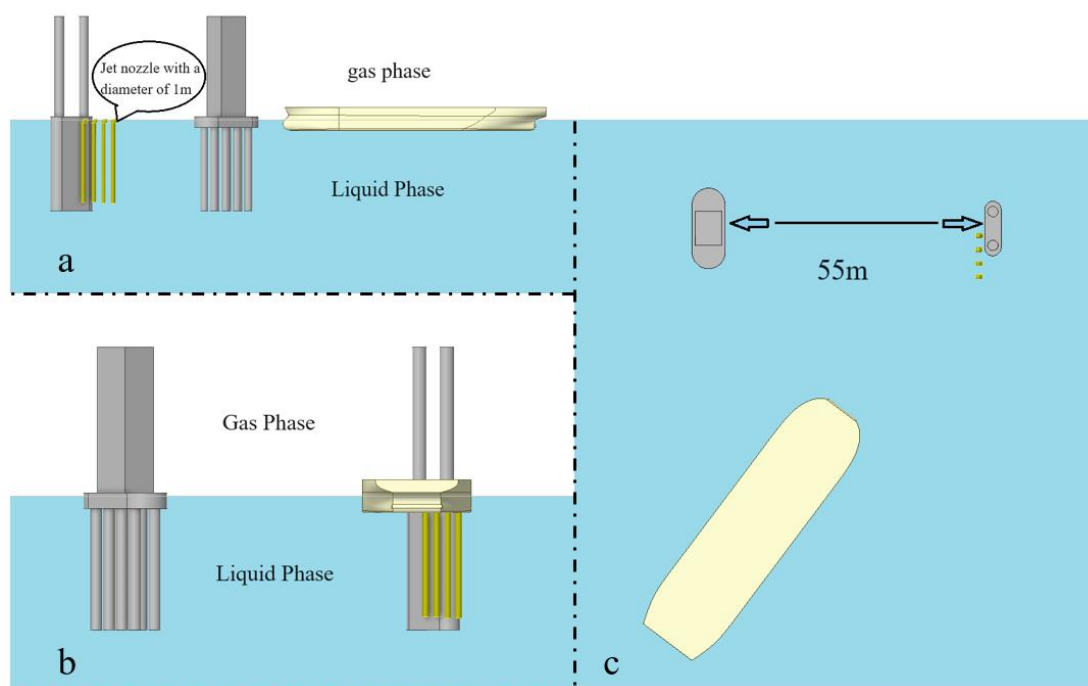


Figure 2. Schematic diagram of fluid domain. (a) Side view of ship; (b) rear view of ship; (c) top view of ship.

2.2. Numerical Simulation Strategy and Boundary Condition Settings

In this paper, the two-phase (water, air) incompressible Reynolds-Averaged Navier–Stokes (RANS) equations were adopted as the governing equations to accurately capture the fluid dynamic during the ship–bridge collision process. For the selection of turbulence models, the Shear Stress Transfer (SST) K- Ω model was employed, which performs well in ship motion simulations. It can accurately handle boundary layer flows and effectively simulate far-field flow characteristics [25]. The Pressure-Implicit with Splitting of Operators (PISO) algorithm was chosen to numerically solve the equations to ensure the accurate and efficient solution of the RANS equations and the continuity equation.

The capture of the free surface was achieved using the Volume of Fluid (VOF) method to accurately simulate the ship waves and fluid dynamics during the ship–bridge collision. The inlet of the computational domain was set as a mixed velocity inlet for air and water, and the outlet was set as a pressure outlet. The upper side and left and right sides of the fluid domain were set as symmetric boundaries to simulate the infinite extension of the flow field. Other components, such as piers and ships, were set as no-slip wall boundary conditions.

2.3. Application of Overset Grid Technology

The large-scale motion of ships in water poses a major challenge in computational fluid dynamics. To effectively simulate this complex process, the overset grid technology was adopted in this paper. This technology not only avoided the negative volume issues caused by dynamic grids, ensuring the stability and accuracy of the calculation process, but also achieved efficient exchange of information data between moving objects (ships) and the fluid domain by dividing them into separate grids (foreground grid and background grid).

2.4. Mesh Generation Strategy and Independence Verification

In this paper, polyhedral meshes were used to finely divide the computational domain, with local densification applied especially around the piers, gas–liquid interfaces, and the ship’s sailing path, as shown in Figure 3. To ensure the accuracy of the calculation results, mesh independence verification was performed. Six sets of meshes with different sizes (see Table 2 for details) were generated, and ship free-floating simulation tests [26] were conducted under different mesh sizes. It was found that when the minimum mesh size is less than 0.38 m, the calculated results of the ship’s interaction with the water flow are basically consistent and less affected by the mesh size, as shown in Figure 4. Considering both computational accuracy and efficiency, a total of 1.66 million meshes with a minimum size of 0.38 m and a maximum size of 3 m were finally selected for subsequent calculations.

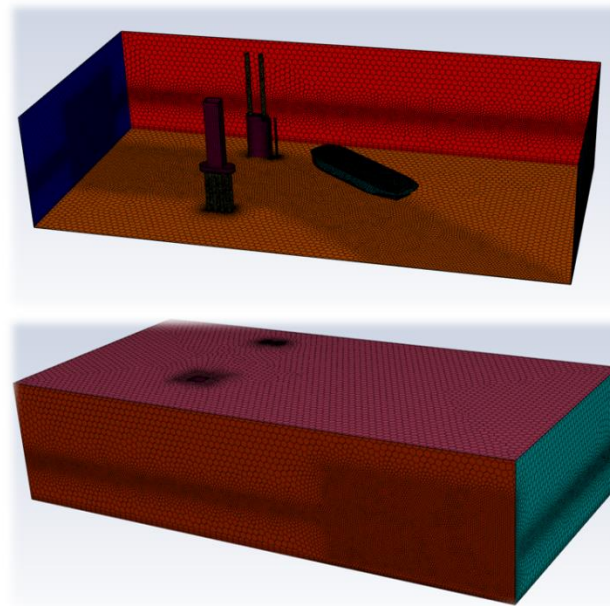


Figure 3. Schematic diagram of mesh generation.

Table 2. Basic mesh parameter information.

Minimum Mesh Size	Grid Number	Face Number
0.46 m	1.15 million	7.36 million
0.43 m	1.35 million	8.88 million
0.40 m	1.55 million	10.15 million
0.38 m	1.66 million	10.83 million
0.35 m	1.88 million	12.31 million
0.32 m	2.46 million	16.24 million

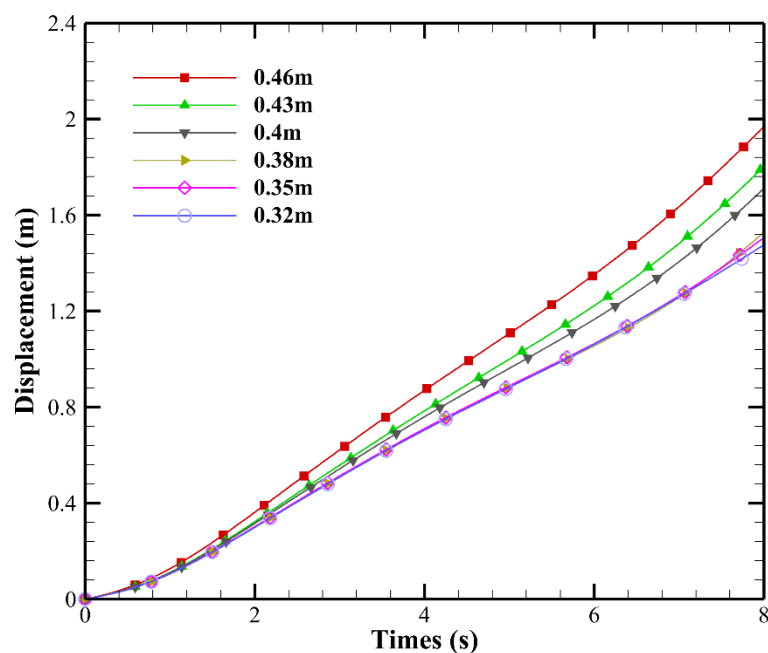


Figure 4. Time-varying curve of surge displacement of freely floating ships under different meshes.

3. Analysis of Numerical Results

3.1. Analysis of the Force on the Steel Plate of the Ship Caused by the High-Pressure Water Jet

In order to effectively change the navigation direction of large-tonnage ships and avoid obstacles such as bridge piers, it is necessary to use high-intensity high-pressure water jets to spray and impact the hull. However, this operation method poses a risk of potential damage to the hull structure. Therefore, in this article, the transient structure and fluent modules in ANSYS 2023 R1 were utilized to perform a fluid–structure interaction analysis in order to assess whether the adopted high-pressure water jet would cause irreversible damage to the hull structure.

To ensure the reliability and broad applicability of the simulation results, the dimensions and strength grade of steel plates under the most unfavorable loading conditions, namely, general-strength structural steel with a length of 18 m, a width of 4.5 m, and a thickness of 0.05 m [27], were selected as the object of this simulation study.

Hull structural steel is subdivided into two major categories based on its minimum yield point: general-strength structural steel and high-strength structural steel [27]. Among them, general-strength structural steel is further classified into four quality grades, namely, A, B, C, and D, which reflect different manufacturing processes and are labeled as CCSA, CCSB, CCSD, and CCSE in the specifications (CCS stands for China Classification Society). The yield strengths of these steels all meet the minimum standard strength of 235 MPa for hull structural steel.

To better simulate the actual operating environment of ships, the outer steel plate of the ship was set to a four-sided fixed state in the static structural section. Additionally, to comprehensively assess the impact of high-pressure water jets on the steel plate, four high-pressure nozzles arranged side by side were set up, each with a diameter of 1 m. The nozzle openings were kept flush with the water surface, and the spacing between adjacent nozzles was set to 2 m. The flow rate of each nozzle was precisely controlled at 11.775 m/s, with a total flow rate of 45 m³/s [28], as shown in Figure 5.

Based on the distance between the steel plate and the high-pressure water jet nozzle, three comparative cases were carefully set up, covering three different distances of 2 m, 4 m, and 8 m. Through detailed calculations and an in-depth analysis, the stress distribution and total deformation data of the steel plate at various distances were successfully

obtained, as shown in Figure 6. It was found that the maximum stress was primarily concentrated at the upper and lower ends of the steel plate, reaching a specific value of 93.2 MPa, as illustrated in Figure 6a, whereas the deformation was primarily concentrated in the middle of the water jet, with a maximum deformation of approximately 1.07 cm, as shown in Figure 6d.

As the distance between the steel plate and the nozzle increased, a significant decrease in both stress and deformation was observed. When the steel plate was placed 4 m away from the nozzle, the maximum stress value was significantly reduced to approximately 62.0 MPa, as shown in Figure 6b; simultaneously, the maximum deformation also dropped to approximately 0.60 cm, as shown in Figure 6e. When the distance between the steel plate and the nozzle further increased to 8 m, the maximum stress value continued to decrease to 34.3 MPa, while the maximum deformation remained minimal, only about 0.40 cm, as shown in Figure 6c and Figure 6f.

These simulation results indicate that by reasonably regulating the jet distance and flow rate of the high-pressure water jet, it is possible to change the ship's course while protecting the pier, and without causing significant damage to the ship's structure. This also suggests that the high-pressure water jet anti-collision method has the potential to become a new, safe, and effective ship navigation and pier protection strategy.



Figure 5. The schematic diagram of steel plate placement in the flow field.

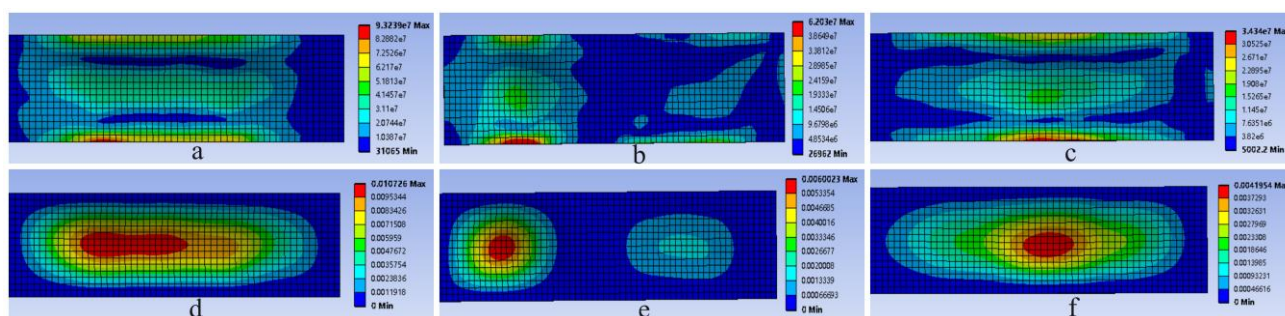


Figure 6. Stress (unit: Pa) distribution of the steel plate at a distance of (a) 2 m, (b) 4 m, (c) 8 m; total deformation (unit: m) at a distance of (d) 2 m, (e) 4 m, (f) 8 m.

3.2. High-Pressure Water Jet Layout and Flow Field Analysis

In this paper, high-pressure nozzles were arranged around the impacted pier, specifically the left pier shown in Figure 2c. The setup parameters of these nozzles strictly adhered to the standards established in detail in Section 3.1. The aim was to ensure that the high-pressure water jets effectively deflect the ship's course without causing any potential damage to the hull, thus safeguarding the safety and effectiveness of the entire system.

Given the specific scenario of the ship's bow colliding with the pier at a 35° angle [29], the precise impact of high-pressure water jet spraying angles on the deflection effect of ships was investigated. Three different spraying angles (0° , -35° , 35°) of water jets were set near the pier, as illustrated in Figure 7. Among them, the 0° condition represented a high-pressure water jet spraying perpendicular to the river flow, where the impact of the vertical water jet would maximize the alteration of the river's flow direction. The -35° condition signified that the high-pressure water jet sprays perpendicular to the river and deflects upstream by 35° , aligning with the ship's impact direction. Theoretically, this condition would cause the ship to be affected by the high-pressure water jet the earliest. Conversely, the 35° condition involved the high-pressure water jet spraying perpendicular to the river and deflecting downstream by 35° , potentially subjecting the ship to a greater turning moment.

When the high-pressure water jet impacted the river channel, the original flow field structure underwent significant changes. Upon being subjected to the action of high-momentum fluid, the ship's original navigation state altered, effectively averting the risk of direct collision between the ship and the bridge [23]. Turbulence is a crucial consideration in waterways, especially when the lateral flow velocity exceeds 0.3 m/s , defining the turbulence width range, which significantly impacts the safe navigation of ships [30]. Therefore, in this paper, a lateral flow velocity greater than 0.3 m/s is used as the criterion for determining the influence area of the high-pressure water jet.

Figure 8 shows the velocity contour and dynamic pressure contour of the high-pressure water jet under different conditions. The velocity contour clearly reveals that the dynamic pressure and flow velocity of the high-pressure water jet reach their maxima at the nozzle outlet. As the water jet expands outward, its velocity and dynamic pressure gradually decrease. The dynamic pressure contour exhibits a similar trend to the velocity contour, with high flow velocities and dynamic pressures concentrated in the central portion of the water jet coverage area, gradually decreasing from the center to the sides. Near the outlet, the maximum dynamic pressure can reach $99,571.4\text{ Pa}$, and the water flow velocity attains approximately 14.8 m/s .

When ships under the three different conditions arrived at the same location, coordinate calculations revealed that the water jet coverage impact range is approximately 30 m long for the -35° condition, 33 m for the 0° condition, and the longest at about 38 m for the 35° condition. The width of the water jet is approximately 10 m for all conditions. Notably, the -35° condition, as an upstream scenario, exhibits a relatively shorter spreading distance of the high-pressure water jet when the ship reaches the same location. Conversely, the 35° condition, being a downstream scenario, demonstrates the farthest spreading distance due to the influence of the river's flow velocity. This causes the tail end of the high-pressure water jet to bend downstream, thereby expanding the interference area of the water jet.

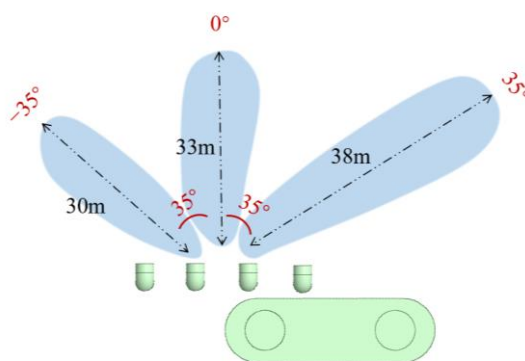


Figure 7. Jet nozzle layout diagram.

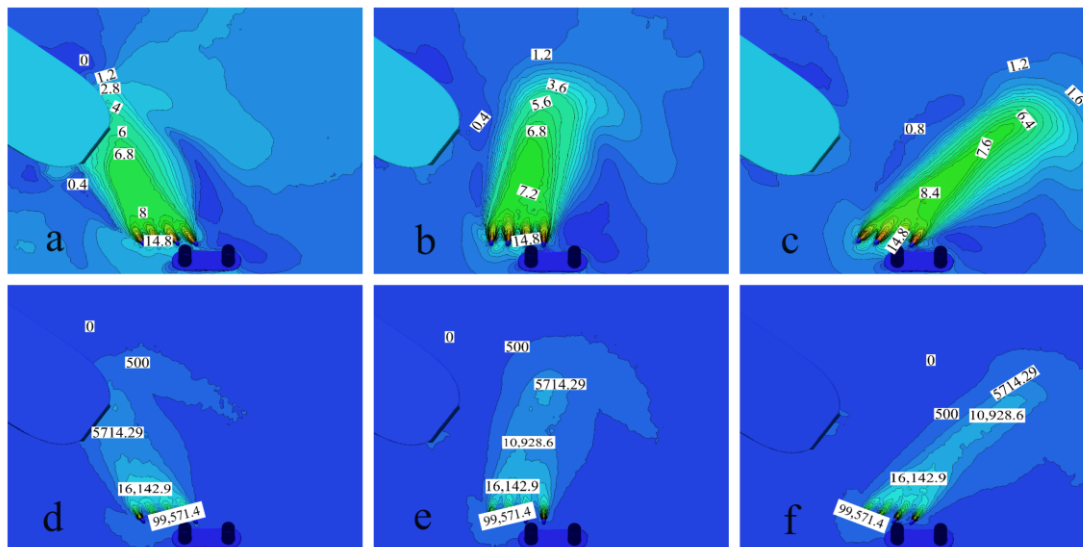


Figure 8. Flow field contours of high-pressure water columns under three working conditions. Velocity (unit: m/s) contour under (a) -35° condition, (b) 0° condition, (c) 35° condition; dynamic pressure (unit: Pa) contour under (d) -35° condition, (e) 0° condition, (f) 35° condition.

3.3. Analysis of Ship Yaw Trajectory under Different Working Conditions

In this paper, the navigation process of a large-tonnage ship approaching the impacted pier was simulated, focusing on the observation of the yaw trajectory of the ship under different working conditions. At the beginning of the experiment, the ship was placed 50 m away from the high-pressure jet nozzle and sailed towards the pier with a deviation angle of 35° and an initial speed of 2.7 m/s. Given the relatively low initial speed, a dragging force of 65 kN was applied to the ship to ensure a stable sailing speed throughout the experiment.

Three different conditions were set up for the experiment to simulate the sailing state of the ship. Figure 9 details the trajectory curves of the ship's center of gravity throughout the entire motion process. It can be seen from the figure that before the ship reaches the coverage area of the high-pressure water jet, its sailing trajectory will be deflected to a certain degree due to the influence of river currents. When the bow reaches the coverage area of the high-pressure water jet, the entire hull will deflect downstream by approximately 2.5 m.

Under the -35° working condition, the ship first came into contact with the impact area of the high-pressure water jet. At this time, the ship was located at the green dashed line scale of 50 m in Figure 9. Since the hull had already deflected slightly, the impact direction of the high-pressure water jet formed a small angle with the ship's forward direction. This small-angle jet impact further steers the ship, as shown in Figure 10a. As the voyage continues, although the ship was still approaching the pier, the deflecting force of the water jet on the hull gradually increased under the continuous high-pressure water jet. This caused the ship to continue steering while its tendency to approach the pier gradually weakened and ultimately began to steer away from the pier. During this process, the minimum distance between the upper right side of the ship and the pier is approximately 8.75 m, as shown in Figure 10d.

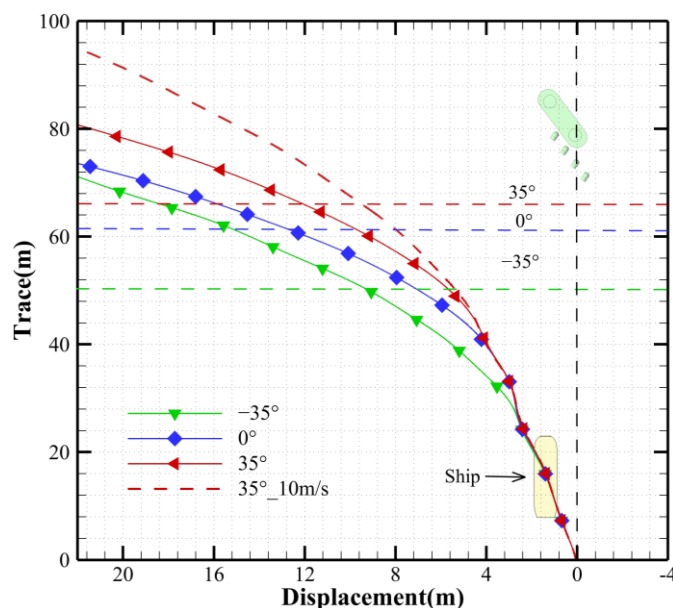


Figure 9. Ship's navigation trajectory through water jet impact area.

Under the 0° working condition, the ship began to be affected by the high-pressure water jet when it reached approximately 62.6 m on the blue dashed line scale in Figure 9. Compared to the -35° working condition, the ship advanced an additional distance of approximately 12.6 m under this condition. During this part of the voyage, the high-pressure water jet hardly interfered with the ship's sailing. Although the high-pressure water jet under the 0° working condition exerted a larger moment on the river water to steer it, the safe space left for the water jet to push away the ship was relatively smaller. When the ship reached the position shown in Figure 10e, the minimum distance between its upper right side and the pier was approximately 5.14 m. Ultimately, the entire hull successfully cleared the impacted pier. However, when the stern passed through the jet nozzle, due to the strong effect of the high-pressure jet source, the bow deflected towards the left-side pier, as shown in Figure 10h. Although the minimum distance between the ship and the pier decreased under this working condition, the ship could still successfully avoid the pier and achieve safe navigation.

Under the 35° working condition, the ship began to be affected by the high-pressure water jet when it reached approximately 66.2 m on the red dashed line scale in Figure 9, as shown in Figure 10c. Compared to the previous two working conditions, the ship was affected by the high-pressure water jet later under this condition, resulting in a smaller space for adjusting its sailing trajectory. After the bow passed through the coverage area of the high-pressure water jet, it arrived at the position shown in Figure 10f. At this point, the minimum distance between the upper right side of the bow and the pier was approximately 2.6 m, which was more urgent compared to the previous two working conditions and posed a greater potential risk to the pier. However, thanks to the strong effect of the high-pressure water jet, the ship was still able to successfully avoid the pier and achieved safe navigation. The moment when the stern passed the pier is shown in Figure 10i.

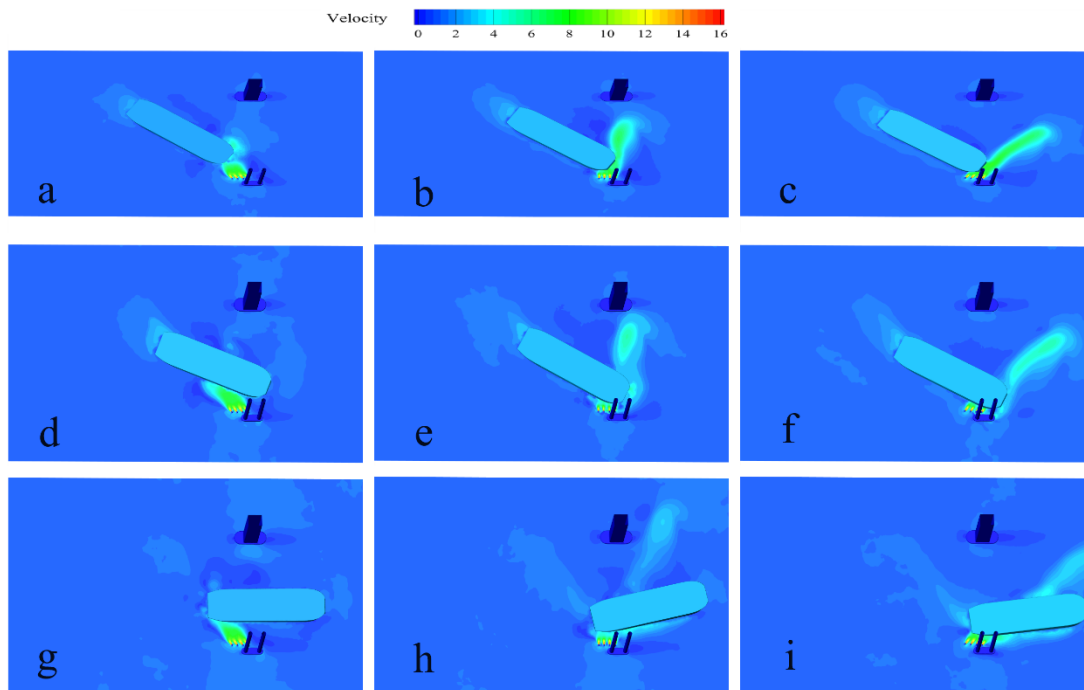


Figure 10. Locations of the ship passing through the high-pressure water jet area. The ship reaching the water jet area under (a) -35° condition, (b) 0° condition, (c) 35° condition; the ship passing over the water jet area under (d) -35° condition, (e) 0° condition, (f) 35° condition; the stern reaching the water jet under (g) -35° condition, (h) 0° condition, (i) 35° condition.

Through an analysis of the first three sets of working conditions, it can be seen that under the condition of maintaining the jetting speed of the high-pressure water jet at 14.8 m/s, ships can effectively and safely avoid the risk of collision with piers. However, during the testing of the 35° working condition, the navigation status of the ship was particularly dangerous, posing a significant potential risk to the pier.

To further clarify the minimum jetting intensity of the high-pressure water jet required to ensure the safety of the ship, the 35° working condition was taken as a benchmark and gradually reduced. Figure 11 clearly shows that when the jetting speed was reduced to 10 m/s, although the minimum distance between the ship and the pier was only about 1.29 m when the ship approached the pier, posing a significant risk to the pier, thanks to the continuous action of the high-pressure water jet, the ship ultimately successfully completed an extreme turn, avoiding collision with the pier. It is worth noting that when the stern of the ship successfully passed the pier, although the bow continued to veer towards the right-side pier and continued to move forward, overall, the ship had safely sailed through the pier area.

Figure 12 details the trend of changes in the yaw angle of the ship under the action of the high-pressure water jet. As can be seen from the figure, due to the influence of the natural flow direction of the river, the bow had already deviated slightly by about 2° before contacting the high-pressure water jet. When the bow first touched the area impacted by the high-pressure water jet, it quickly veered to the left under the significant influence of the force moment generated by the water jet. Among them, the ship under the -35° working condition turned earlier than under other conditions. However, due to the small angle between the water jet and the hull, the turning moment acting on the ship was relatively small, resulting in a relatively gradual increase in its yaw angle. In contrast, under the 0° working condition, the impact direction of the high-pressure water jet was perpendicular to the flow direction, causing the maximum impact on the flow direction of the river water, leading to the most rapid increase in the yaw angle of the ship in this area. The accumulated yaw angle when exiting the area reached a maximum of 55° . As for the

35° working condition, although the ship was subjected to a large turning moment from the impact of the water jet, as the water jet was sprayed downstream, when the ship turned to a certain angle, the force moment of the water jet on the ship rapidly decreased, ultimately resulting in a yaw angle that was larger than under the -35° working condition but smaller than under the 0° working condition. In the working condition with a reduced jetting flow rate of the water jet, due to insufficient power of the water jet, the increase in the yaw angle of the ship was the slowest, and the final yaw angle was also the smallest.

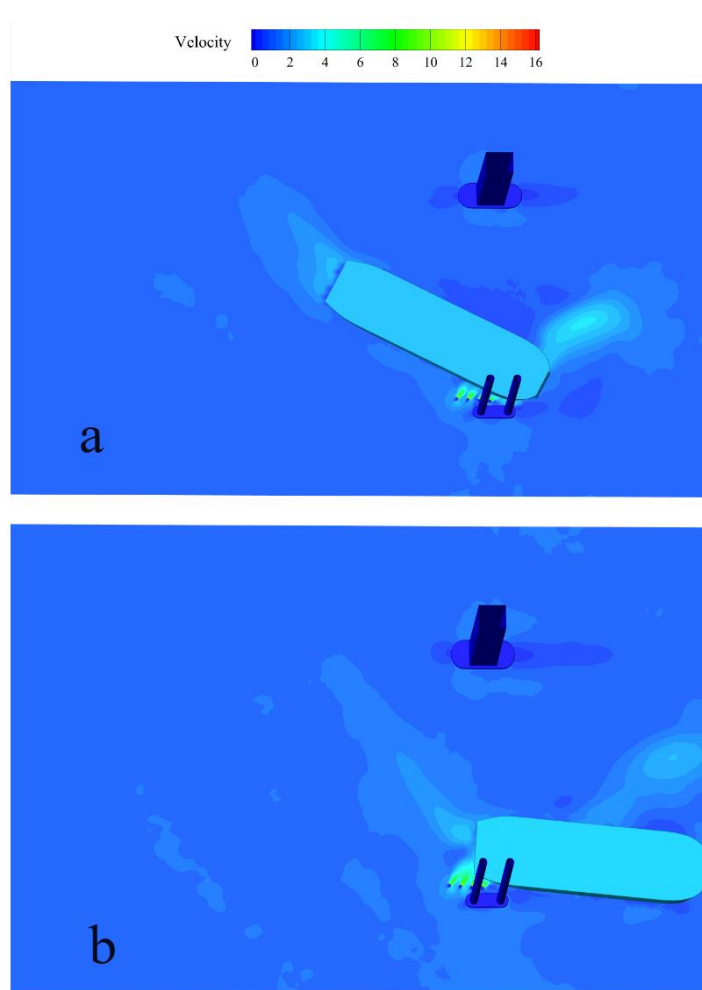


Figure 11. Location of ship under 35° condition with jetting speed of 10 m/s: (a) the ship reaching the water jet area; (b) the stern reaching the water jet area.

Based on the experimental results of the four working conditions mentioned above, the following conclusions can be drawn: the high-pressure water jet collision avoidance method is practical and effective for large-tonnage ships. Under various working conditions, the ships exhibited significant lateral displacement and yawing, effectively correcting their off-course situations. After being influenced by the high-pressure water jet, the lateral displacement of the ships reached more than 22 m. Additionally, due to differences in the impact area and duration of the high-pressure water jet under different working conditions, the ship under the -35° working condition was first affected by the water jet and was affected for a longer duration, providing sufficient time for the ship to turn away from the pier. Under the 0° and 35° working conditions, although the force moment of the water jet on the ship was greater, due to the later timing of the impact, the ship had limited space and time to adjust its course. Although it ultimately succeeded in avoiding the pier, it was clearly very close to it, posing a certain risk of collision. This finding suggests that

compared to the force moment of the water jet, the duration of its impact is more critical for collision avoidance effectiveness. When configuring the same high-pressure water jet, it is advisable to maximize the duration and range of the water jet's impact on the ship to allow the ship to start turning and decelerating earlier.

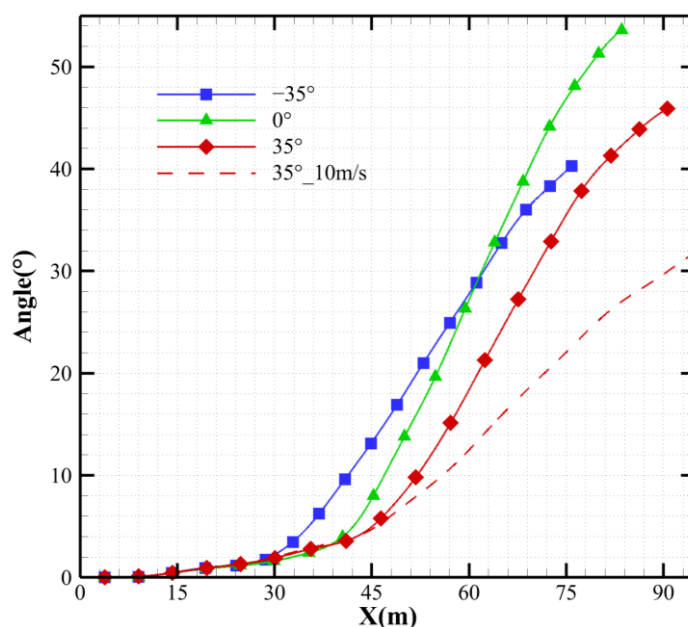


Figure 12. Ship steering curve under different working conditions.

It is worth mentioning that under the most unfavorable 35° working condition, when the jetting speed of the high-pressure water jet was reduced to about 10 m/s, the ship was still able to successfully avoid the pier. This finding indicates that there is still some room for optimization in the configuration of the high-pressure water jet. If a higher-power jetting device can be provided, it will be possible to protect the safety of piers while avoiding collisions with larger-tonnage ships.

When facing the emergency situation of large-tonnage ships losing control, relying solely on the ship's own engine braking and rudder adjustment is often difficult to effectively avoid collisions. Therefore, from the perspective of the lateral displacement and yaw angle of the ship in this simulated experiment, the high-pressure water jet collision avoidance method has been proven as theoretically feasible. Through the impact of high-pressure water flow, it can provide a huge steering force for the uncontrolled ship, enabling it to completely avoid the pier and achieve "zero damage" between the ship and the bridge.

3.4. Impact of High-Pressure Water Jet on Ship Movement

When a ship encounters the instant impact of a high-pressure water jet, it will face the jet impact from the front or side depending on different working conditions. This impact will generate significant water waves at the bow position, further affecting the resistance of the hull. Ship resistance mainly includes wave-making resistance and viscous pressure resistance. Wave-making resistance originates from the water waves generated during hull propulsion, while viscous pressure resistance results from the viscosity of water molecules on the hull surface. The formation of these water waves undoubtedly increases the resistance of the ship, resulting in a significant reduction in ship speed, as

shown in Figure 13. Specifically, when the bow touched the area impacted by the high-pressure water jet, the ship speed decreased more significantly.

By comparing different working conditions, it was found that when the working condition was 35° and the flow rate was 10 m/s, the decrease in ship speed was relatively small, fluctuating only around 2.7 m/s. This may be because under this condition, the high-pressure water jet mainly impacts the side of the ship, and the flow rate of the water jet is relatively small. Therefore, the impact range of the water jet on the bow is relatively small, resulting in less wave-making resistance that can be almost ignored. However, when the water jet tilted upstream at an angle of -35° , the decrease in ship speed was the most significant, rapidly dropping from 2.55 m/s to approximately 1.7 m/s and remaining stable until the middle and tail sections of the ship passed through the area impacted by the high-pressure water jet, where the speed continued to decrease. This phenomenon further explains why, as mentioned in Section 3.3, under this working condition, the ship can maintain a larger safety distance from the pier. This is mainly because, under this condition, the high-pressure water jet not only deflects the ship but also reduces its speed through the generation of reactive force, effectively preventing the ship from approaching the pier.

In addition, ships generate a series of waves, known as Kelvin waves, during navigation, which often leads to the phenomenon of ship pitching. The amplitude of pitching directly affects the stability of the ship's movement and the comfort of passengers. Figure 14 shows the variation curves of ship pitching under different working conditions. As can be seen from the figure, regardless of the working condition, when the ship's center of gravity passed through the area impacted by the high-pressure water jet, its pitching amplitude decreased. Taking the -35° working condition as an example, before the ship's center of gravity entered the area impacted by the high-pressure water jet, its pitching peak was 0.1° , the trough was -0.75° , and the difference between the peak and the trough was 0.85° , with a wavelength of approximately 10.5 m. However, when the ship's center of gravity entered the water jet area (approximately within a range of 50 m), its pitching value decreased to -0.2° , the trough was -0.6° , and the difference between the peak and the trough reduced to 0.4° , while the wavelength remained approximately 10.5 m. This indicates that under the action of the high-pressure water jet, the peak pitching value of the ship decreases, but the period of the wavelength does not change significantly. Therefore, by interfering with ship navigation through high-pressure water jet spraying, it can not only effectively deflect the ship away from the pier, but the impact of the water jet on the stability of the ship's movement and passenger comfort is relatively small.

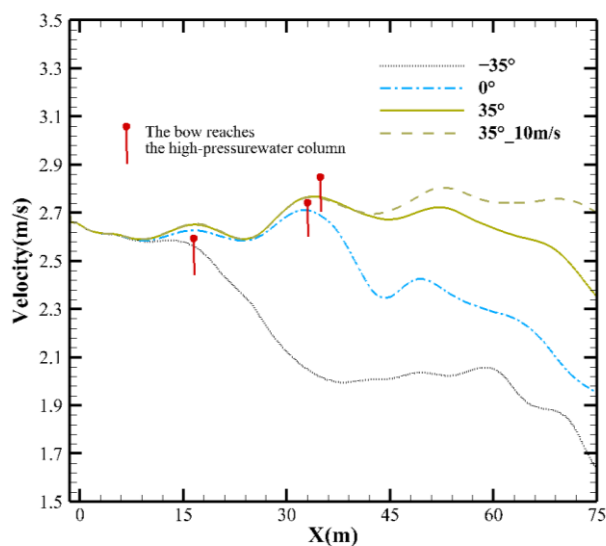
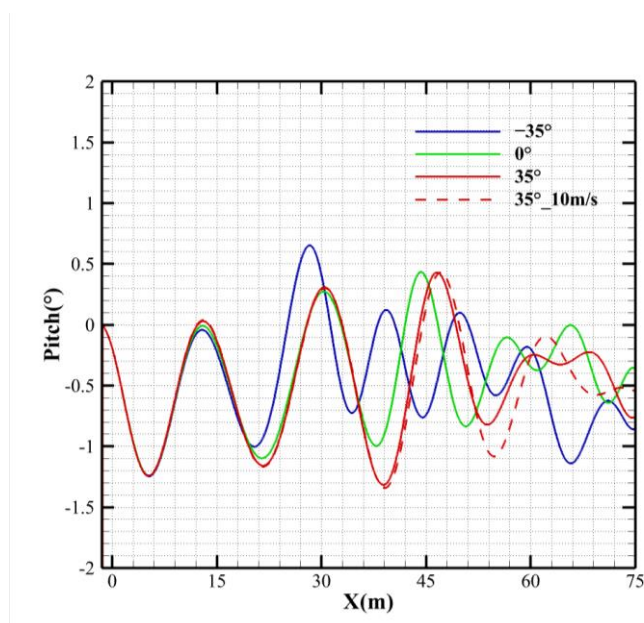


Figure 13. Ship speed variation curve.**Figure 14.** Curves of ship pitching under different working conditions.

4. Conclusions

Through a fluid–structure interaction analysis, the stress conditions of ship steel plates under the action of high-pressure water jets have been investigated. The results revealed that, despite the maximum deformation of approximately 1 cm occurring in the middle part of the Q235 steel plate, which was located 2 m away from the nearest end of the high-pressure jet nozzle, this deformation fell within an acceptable range, unlikely to cause permanent damage to the steel plate. This finding provides strong support for the safety of high-pressure water jets in practical applications.

Moreover, it was also found that the spraying angle of the high-pressure water jet had a significant impact on the deflection effect of the ship. Simulation results indicate that when the water jet nozzle is aligned exactly opposite to the direction of the ship's impact (i.e., the -35° working condition), the high-pressure water jet exerts the longest duration of force on the ship, achieving an optimal collision avoidance effect and effectively maintaining a minimum safe distance of approximately 8.75 m between the ship and the pier. This discovery provides important guidance for optimizing the high-pressure water jet collision prevention system, as precise control of the ship's trajectory can be achieved by adjusting the water jet spraying angle appropriately.

It is worth noting that although the high-pressure water jet can significantly change the ship's sailing direction, its impact on the ship's stability and passenger comfort is relatively small. This characteristic makes the high-pressure water jet collision prevention method more feasible in practical applications, minimizing the impact on the ship's normal operations while ensuring safety.

In summary, the effectiveness of high-pressure water jets in changing the sailing direction of large-tonnage ships and avoiding obstacles was verified in this study through a simulation analysis. And the impact on the stress of ship steel plates and the navigation status were also comprehensively analyzed. The research results demonstrate that high-pressure water jet technology has tremendous practical application potential and can provide new solutions for waterway transportation safety.

Considering the ship tonnage, impact speed, and angle of the Lixinsha accident, it has been demonstrated that this technology could effectively avoid collisions in ships weighing 2200 tons or less. In future work, we will further explore the applicability of

high-pressure water jet collision avoidance technology by considering the range of ship tonnage and accident speed commonly seen in ship–bridge collisions in China’s inland rivers. Meanwhile, under the current jet flow conditions, we will investigate the maximum ship tonnage suitable for the HPWJI method. We anticipate that through continuous research and optimization, this technology can be better applied in practical scenarios, making greater contributions to enhancing the safety of waterway transportation.

Author Contributions: Conceptualization, J.C.; methodology, J.C. and M.D.; software, X.W.; formal analysis, X.W.; investigation, X.W. and J.H.; resources, X.W. and J.H.; data curation, X.W. and H.W.; writing—original draft, J.C.; writing—review & editing, J.C., X.W., J.H., H.W. and M.D.; supervision, M.D.; project administration, M.D.; critical review, J.C. and M.D. All authors have read and agreed to the published version of the manuscript.

Funding: This research received no external funding.

Data Availability Statement: The data presented in this study are available on request from the corresponding author.

Conflicts of Interest: The authors declare no conflict of interest.

References

1. Wang, F.; Chang, H.-J.; Ma, B.-H.; Wang, Y.-G.; Yang, L.-M.; Liu, J.; Dong, X.-L. Flexible Guided Anti-Collision Device for Bridge Pier Protection against Ship Collision: Numerical Simulation and Ship Collision Field Test. *Ocean Eng.* **2023**, *271*, 113696. <https://doi.org/10.1016/j.oceaneng.2023.113696>.
2. Irhayyim, A.; Gunaratne, M.; Fioklou, A. Assessment of Scoured Bridges Subjected to Ship Impact. *Structures* **2022**, *36*, 635–649. <https://doi.org/10.1016/j.istruc.2021.12.023>.
3. Kang, L.; Magoshi, K.; Ge, H.; Nonaka, T. Accumulative Response of Large Offshore Steel Bridge under Severe Earthquake and Ship Impact Due to Earthquake-Induced Tsunami Flow. *Eng. Struct.* **2017**, *134*, 190–204. <https://doi.org/10.1016/j.engstruct.2016.12.047>.
4. Perera, L.P.; Guedes Soares, C. Collision Risk Detection and Quantification in Ship Navigation with Integrated Bridge Systems. *Ocean Eng.* **2015**, *109*, 344–354. <https://doi.org/10.1016/j.oceaneng.2015.08.016>.
5. Shen, Z.L. Review on Research Progress of Anti-Collision Equipment for Bridge Protection. *Transp. Sci. Technol.* **2015**, 73–76. <https://doi.org/10.3963/j.issn.1671-7570.2015.03.024>. (In Chinese)
6. Fang, Z.X.; Su, P.H.; Xu, B.J.; He, X.Y.; Yang, K. The Design of a Multi-Level Active Anti-Collision Warning Platform for Cross-Sea Bridges. *Port Technol.* **2023**, *9*, 33–38.
7. Zhang, H.Z.; Chen, H.; Zhou, L. Study of Bridge Anti-Collision System Base on Video Surveillance Technology. *J. Shang Hai Jiao Tong Univ.* **2011**, *45*, 93–96. (In Chinese)
8. Zhao, J. Risk Analysis of Bridge Ship Collision and Application of Anti-Collision System. *World Transp.* **2022**, *10*, 9–10. (In Chinese)
9. Guo, Z.J.; He, X. Research on Scanning-Photoelectric Warning System Based on Real-Time Image Processing. Ph.D. Thesis, Chinese Academy of Science, Beijing, China, 2012.
10. Rothmund, S.V.; Tengesdal, T.; Brekke, E.F.; Johansen, T.A. Intention Modeling and Inference for Autonomous Collision Avoidance at Sea. *Ocean Eng.* **2022**, *266*, 113080. <https://doi.org/10.1016/j.oceaneng.2022.113080>.
11. Du, L.; Valdez Banda, O.A.; Goerlandt, F.; Huang, Y.; Kujala, P. A COLREG-Compliant Ship Collision Alert System for Stand-on Vessels. *Ocean Eng.* **2020**, *218*, 107866. <https://doi.org/10.1016/j.oceaneng.2020.107866>.
12. Tran, H.A.; Johansen, T.A.; Negenborn, R.R. A Collision Avoidance Algorithm with Intention Prediction for Inland Waterways Ships. *IFAC-PapersOnLine* **2023**, *56*, 4337–4343. doi:10.1016/j.ifacol.2023.10.1805.
13. Terndrup Pedersen, P.; Zhang, S. On Impact Mechanics in Ship Collisions. *Mar. Struct.* **1998**, *11*, 429–449. [https://doi.org/10.1016/S0951-8339\(99\)00002-7](https://doi.org/10.1016/S0951-8339(99)00002-7).
14. Mei, J.; Liu, J.; Zhang, M.; He, Z.; Huang, W. Mechanical Behaviors of the Carbon Fiber Reinforced X-Core Sandwich Structure under the Dynamic Compression. *Compos. Struct.* **2023**, *303*, 116341. <https://doi.org/10.1016/j.compstruct.2022.116341>.
15. Mei, J.; Liu, J.; Zhang, M.; Huang, W. Experimental and Numerical Study on the Ballistic Impact Resistance of the CFRP Sandwich Panel with the X-Frame Cores. *Int. J. Mech. Sci.* **2022**, *232*, 107649. <https://doi.org/10.1016/j.ijmecsci.2022.107649>.
16. Chen, P.; Sun, B. Simulation of Crooked Plate Energy Absorption Structure under Impact. *AMS* **2022**, *38*, 521429. <https://doi.org/10.1007/s10409-021-09019-x>.
17. Wan, Y.; Liu, Y.; Hu, C.; Yao, J.; Wang, F.; Yang, B. The Failure Mechanism of Curved Composite Laminates Subjected to Low-Velocity Impact. *AMS* **2023**, *39*, 423113. <https://doi.org/10.1007/s10409-023-23113-x>.
18. Su, X.; Lin, W.J.; Chen, W.; Pan, J.; Li, X.B. Analysis of Performance and Influencing Factors of the Ellipsoidal Anti-Collision Airbag. *J. Wuhan Univ. Technol. Transp. Sci. Eng.* **2023**, 1–11. Available online: <https://kns.cnki.net/kcms2/detail/42.1824.U.20230705.1953.028.html> (accessed on 25 June 2024). (In Chinese)

19. Yan, H.; Jia, E.; Fang, H.; Zhu, L.; Zhang, X.; Dai, Z. Impact Dynamics Analyses on an Innovative Fiber-Reinforced Rubber Composite Bumper System for Bridge Protection. *Thin-Walled Struct.* **2024**, *195*, 111331. <https://doi.org/10.1016/j.tws.2023.111331>.
20. Zhu, L.; Liu, W.; Fang, H.; Chen, J.; Zhuang, Y.; Han, J. Design and Simulation of Innovative Foam-Filled Lattice Composite Bumper System for Bridge Protection in Ship Collisions. *Compos. Part B Eng.* **2019**, *157*, 24–35. <https://doi.org/10.1016/j.compositesb.2018.08.067>.
21. Fang, H.; Mao, Y.; Liu, W.; Zhu, L.; Zhang, B. Manufacturing and Evaluation of Large-Scale Composite Bumper System for Bridge Pier Protection against Ship Collision. *Compos. Struct.* **2016**, *158*, 187–198. <https://doi.org/10.1016/j.compstruct.2016.09.013>.
22. Lian, X.-G.; Lu, L.-X.; Pan, L. Investigation of Energy Absorption Characteristics of Circular Paper Tubes under Axial Impact Loading. *Int. J. Impact Eng.* **2022**, *165*, 104210. <https://doi.org/10.1016/j.ijimpeng.2022.104210>.
23. Chen, J.; Wei, X.; Huang, J.; Fu, D.; Wang, H.; Zhou, Z. Numerical Evaluation of A New High Pressure Water Jet Interference Method for Bridge Pier Protection against Vessel Collision. *Acta Mech. Sin.* **2024**, *38*. <https://doi.org/10.1007/s10409-024-24069-x>.
24. Tian, H.N. Analysis of Collision Protection Performance of Composite Anti-Collision Devices for Lixinsha Bridge in Guangzhou. *Bridge Constr.* **2023**, *53*, 66–73.
25. Shen, Z.; Ye, H.; Wan, D. Motion Response and Added Resistance of Ship in Head Waves Based on RANS Simulations. *Chin. J. Hydrodynamics* **2012**, *27*, 621–633.
26. Ye, X.; Fan, W.; Sha, Y.; Hua, X.; Wu, Q.; Ren, Y. Fluid-Structure Interaction Analysis of Oblique Ship-Bridge Collisions. *Eng. Struct.* **2023**, *274*, 115129. <https://doi.org/10.1016/j.engstruct.2022.115129>.
27. Structural Specification for Container Ship. China Classification Society, (CCS): Beijing, China, 2022. Available online: <https://www.ccs.org.cn/ccswz/specialDetail?id=202208091074947939> (accessed on 25 June 2024). (In Chinese).
28. Li, X.H.; Zhu, Y.Q.; Nie, S.L. The Overview of Development and Research for Waterjet Propulsion. *Chin. Hydraul. Pneum.* **2007**, *1–4*. <https://doi.org/10.3969/j.issn.1000-4858.2007.07.001>. (In Chinese)
29. Guangdong Maritime Safety Administration. *Investigation Report on the Accident of the Ship “Lianghui 688” Colliding with Lixinsha Bridge in Guangzhou on February 22nd*; Guangdong Maritime Safety Administration: Guangzhou, China, 2024.
30. Zhang, Y.; Tan, Z.; Liu, J.; Li, X. Effect of Pier Anti-Collision Facilities on Turbulence Width. *J. Chong Qing Jiao Tong Univ. Nat. Sci.* **2023**, *42*, 22–28.

Disclaimer/Publisher’s Note: The statements, opinions and data contained in all publications are solely those of the individual author(s) and contributor(s) and not of MDPI and/or the editor(s). MDPI and/or the editor(s) disclaim responsibility for any injury to people or property resulting from any ideas, methods, instructions or products referred to in the content.